PSFC/JA-01-13

Phase Contrast Imaging of Ion Bernstein and Fast Waves in Alcator C-Mod

E. Nelson-Melby, A. Mazurenko, M. Porkolab,
P.T. Bonoli, S.J. Wukitch

August 2001

Plasma Science and Fusion Center
Massachusetts Institute of Technology
Cambridge, MA 02139 USA

This work was supported by the U.S. Department of Energy, Cooperative Grant No. DE-FC02-99ER54512. Reproduction, translation, publication, use and disposal, in whole or in part, by or for the United States government is permitted.

Submitted for publication in proceedings of *14th Topical Conference on Radio Frequency Power in Plasmas* (Oxnard, CA, 7-9 May 2001).

Phase Contrast Imaging of Ion Bernstein and Fast Waves in Alcator C-Mod*

E. Nelson-Melby, A. Mazurenko, M. Porkolab,
P.T. Bonoli, S.J. Wukitch

MIT PSFC, Cambridge, MA 02139 U.S.A

Abstract. Direct observation of ICRF (~80 MHz) waves ($k_\perp \simeq 0.5\,cm^{-1} - 10\,cm^{-1}$) is now possible in Alcator C-Mod using an optical heterodyne technique on the Phase Contrast Imaging (PCI) system, which uses a CO_2 laser to observe electron density fluctuations. The PCI observations are vertical chord averages, so the full-wave ICRF code TORIC[1] has been used to simulate the wave fields in these plasmas to aid in interpretation. Mode-converted ion Bernstein waves (IBW) in plasmas composed of H, D and ^{3}He at 6 T have been observed at both high (1 MA) and low (400 kA) current. The fast magnetosonic wave launched from the low-field side has been observed in high density ($\sim 5\times10^{20}\,m^{-3}$) D(H) plasmas with off-axis ICRH at 4.5 T. Comparison between PCI measurements and code results are presented. The measured wave numbers are in good agreement with the local dispersion relations for both types of waves.

INTRODUCTION

Electron density fluctuations directly associated with Ion Bernstein Waves (IBW)[2] and Fast Magnetosonic Waves (FW)[3] have been measured in the Alcator C-Mod tokamak with a Phase Contrast Imaging (PCI) diagnostic. The spatial structure and wavelength of the waves can be derived from the PCI results.

The FW can be launched at high power in large magnetic fusion experiments and damp effectively in the hottest regions of the plasma, producing central heating. IBWs can exist between any pair of cyclotron resonances and their harmonics. They also can damp effectively in present and future magnetic fusion devices, either by electron Landau damping or ion cyclotron (harmonic) damping. Localized IBW damping on electrons can be used for current drive, current profile control, and/or flow drive accompanied by enhanced confinement. Considerable theoretical effort has been devoted to understanding both of these waves in hot fusion plasma experiments, and the PCI data can help validate and test ICRF theory and codes concerning fast wave propagation, damping, and mode conversion to an IBW.

Previous attempts to measure ion Bernstein waves directly in magnetic fusion experiments have usually relied on small-angle laser scattering[4-8]. Fast magnetosonic waves have been more difficult to measure, but magnetic probes[9] and reflectometry[10] have succeeded in revealing the spatial structure of the FW inside a tokamak.

PHASE CONTRAST IMAGING

Also referred to as "internal reference interferometry", Phase Contrast Imaging[11,12] relies on the interference of scattered and appropriately phase-shifted unscattered radiation passing through a phase object, such as a plasma with electron density fluctuations causing the scattering. The PCI system on the Alcator C-Mod tokamak uses a 10.6 μm wavelength CO_2 laser, expanded to a width of 15 cm, passing through the central portion of a 42 cm wide plasma. After passing through the plasma and the rest of the system, the laser light is imaged onto a 12 element HgCdTe photoconductive linear array. The detectors are sensitive up

to 10 MHz, and high-pass filters are used to pass through only $\gtrsim 2$ kHz fluctuations, thus avoiding a large steady state signal and the noisy lowest frequency range of fluctuations. There are also 500 kHz low-pass filters to avoid aliasing, as the voltages from the detectors are sampled and digitized at 1 MHz (500 KHz Nyquist frequency), so the system is sensitive to frequencies from 2 to 500 kHz. The longest wavelength that can be effectively imaged is approximately the beam width, thus setting a lower bound for detectable k numbers of about 0.4 cm^{-1}. Short wavelength detection is limited in practice by the number of channels and their spacing, setting an upper limit in k between $5 - 10$ cm^{-1}, depending on how large a portion of the beam is imaged on the 12 detectors.

If the laser beam encounters a density perturbation which is purely sinusoidal and propagating perpendicular to the beam, the laser electric field can then be represented by a uniform intensity background with some phase variations and can be decomposed into three plane waves: the unscattered wave, and left and right scattered waves of small amplitude. After leaving the plasma the laser beam is focussed by an off-axis parabolic mirror onto a reflective plate with a partially reflecting narrow groove where the main beam spot is focussed. The groove is $\lambda/8$ deep (1.325 μm) so that the main beam travels $\lambda/4$ (90° of phase) farther than the scattered portions of the beam. The extra distance travelled causes the contribution of the scattered light to be in phase with the unscattered light when imaged on the detectors, converting original phase variations of the beam electric field into intensity variations. The system thus measures electron density fluctuations, line-integrated along vertical chords.

In order to detect electron density fluctuations at the RF frequency of approximately 80 MHz, the laser is modulated in intensity. This is done by splitting the beam, upshifting one half and downshifting the other using acousto-optical frequency shifters, and then recombining the two halves into one beam before entering the plasma. The modulation frequency is chosen to be a few hundred kHz different from the RF frequency, for example 80.3 MHz. When the 80 MHz signal in the plasma is illuminated by the 80.3 MHz modulated laser, the image intensity (which is the product of both) reveals a 300 kHz beat oscillation, the frequency at which the detectors see the signal.

EXPERIMENTAL MEASUREMENTS

Fast Magnetosonic Wave

The FW in C-Mod is launched from a two-strap (0,π) antenna on the low-field-side at 93 cm major radius. The wave has been detected for the first time with the PCI diagnostic for D(H) plasmas at 4.5 Tesla, placing the H minority resonance 12 cm to the high-field-side of center. These shots are often accompanied by an internal transport barrier[13,14] so the central density rises to as much as $6 \times 10^{20}\, m^{-3}$. The PCI laser passes directly in front of the E-port ICRF antenna (80.0 MHz) but the FW has not been observed when the E-port antenna is energized. This is to be expected for an antenna when the straps are out of phase – there should be a node of the electric field along a line of points equidistant from the straps. The D-port antenna (80.5 MHz) is located 36° or 58 cm away from the PCI laser. When the D-port antenna is energized, the fast wave has been detected (**Fig. 1**). The magnitude of the measured wave number from a 2-D Fourier transform of the raw data is $1.7 \pm 0.9\, cm^{-1}$, in fairly good agreement with the fast wave dispersion relation for these plasmas.

Both positive and negative k_R (phase velocity towards or away from the antenna) are observed, often with different intensities. In fact, during a density

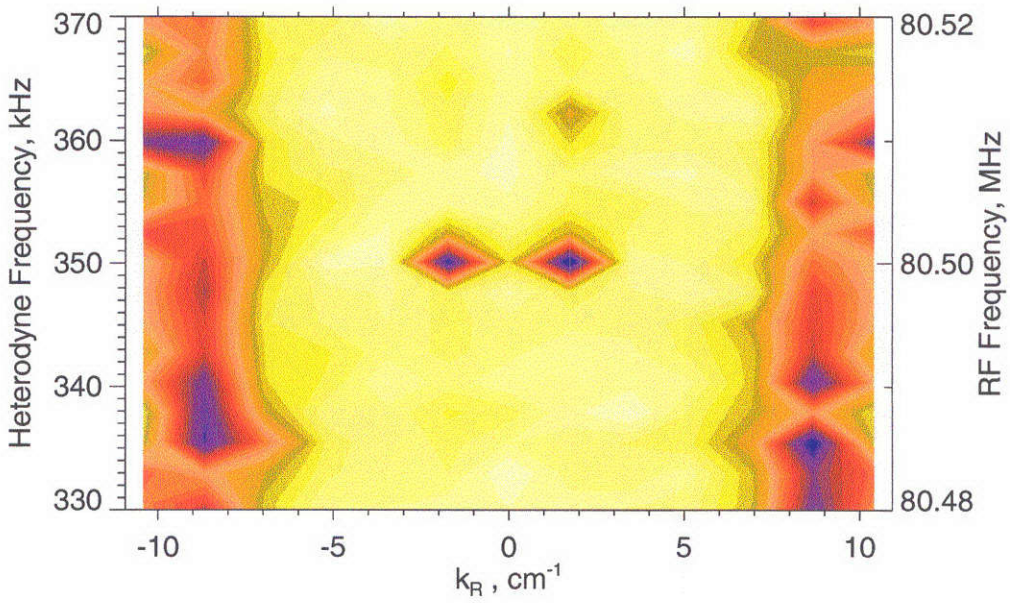

FIGURE 1. Fast Wave observation at $k_R = \pm 1.7\, cm^{-1}$.

ramp, the intensity of the reflected wave (positive k_R) was first stronger than, then comparable, and finally weaker than the forward wave (negative k_R), as seen in **Fig. 2**.

The local fluctuating density near the center in these high density shots at 4.5 T should be roughly a factor of 3 – 5 times stronger than in the more typical C-Mod D(H) scenarios at 5.4 T and central densities of $2-3\times10^{20}m^{-3}$ for the same input power from the antenna (constant Poynting flux), since the RF fluctuating density for the fast wave is approximately given by

$$n_{e1} \propto (n_{e0}^{1.25}/B_{tor}^{1.5})\sqrt{P_{RF}}.$$

In lower density shots, the wavelength may be too long to be resolved by the PCI diagnostic. If so, then at high density the wavelength should be short enough to come within the range of resolvable k numbers (0.4 to 10 cm^{-1}). The FW may also be seen in this scenario but not in others because of refraction effects enhanced by the strong density gradients guiding the FW power from D-port through the PCI window (at E-port) only under certain conditions. 3-D full wave code simulations with TORIC[1] using a full spectrum of toroidal mode numbers suggests that some combination of refraction and focussing may be factors in allowing the FW to be imaged in these peaked density profile shots.

Mode-Converted Ion Bernstein Waves

In order to observe mode-converted IBWs near an ion-ion hybrid layer with the PCI viewing the center of the plasma, experiments were carried out with plasmas consisting of comparable amounts of D, ^{3}He, and H at 5.8 Tesla. This places the mode conversion region to the high-field-side relative to the center, with the exact location and mode conversion efficiency depending sensitively on the exact species mix. The efficiency also varies with the density and density profile.

The main results of the mode-converted IBW experiments are that PCI signal structure with wave numbers from +5 to +10 cm^{-1} (phase velocity toward the

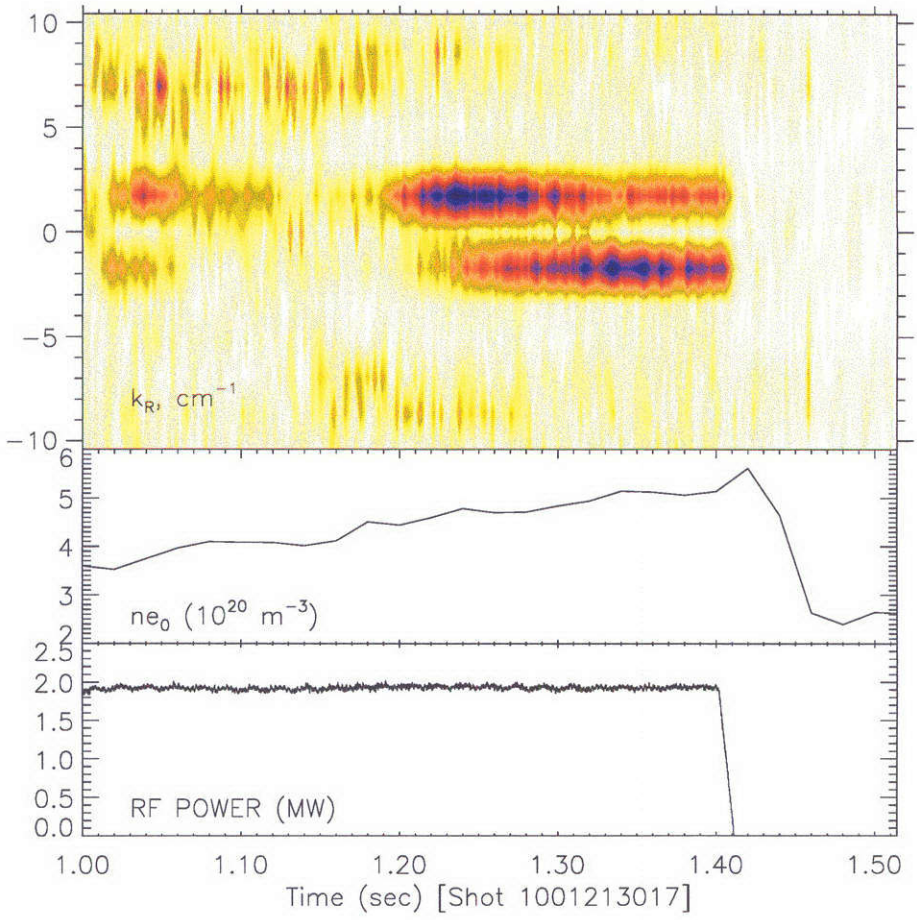

FIGURE 2. Fast Wave k spectrum during density ramp (with constant RF power).

antenna, showing the backward wave nature of the IBW) have been seen in these mixed species plasmas. A 2-D Fourier transform of the raw PCI data where an IBW was observed is shown in **Fig. 3**.

The amplitude of the density fluctuations should scale linearly with the RF electric field, or as the square root of RF power. For a power ramp where other plasma parameters remained roughly constant, this expected behavior was verified as shown in **Fig. 4**.

The detailed structure of the signal intensity across major radius depends sensitively on the exact species mix and the density and density profile, and to a lesser extent on the temperature and magnetic field. For example, during an RF power ramp where the density is increasing (probably changing the ion species ratio as well) the structure of the IBW signal exhibited peaks in intensity, separated by about 1 cm, as shown in **Fig. 5**.

RF FULL WAVE MODELLING

Since the PCI measurements are one-dimensional line-integrated measurements of an inherently 3-D wave field structure, interpretation of the results can be difficult. The separation between peaks in intensity of 1 to 2 cm is longer than the typical IBW wavelength, yet shorter than the FW wavelength. However, full-wave modelling has shown a possible explanation for the spatial scale of these structures.

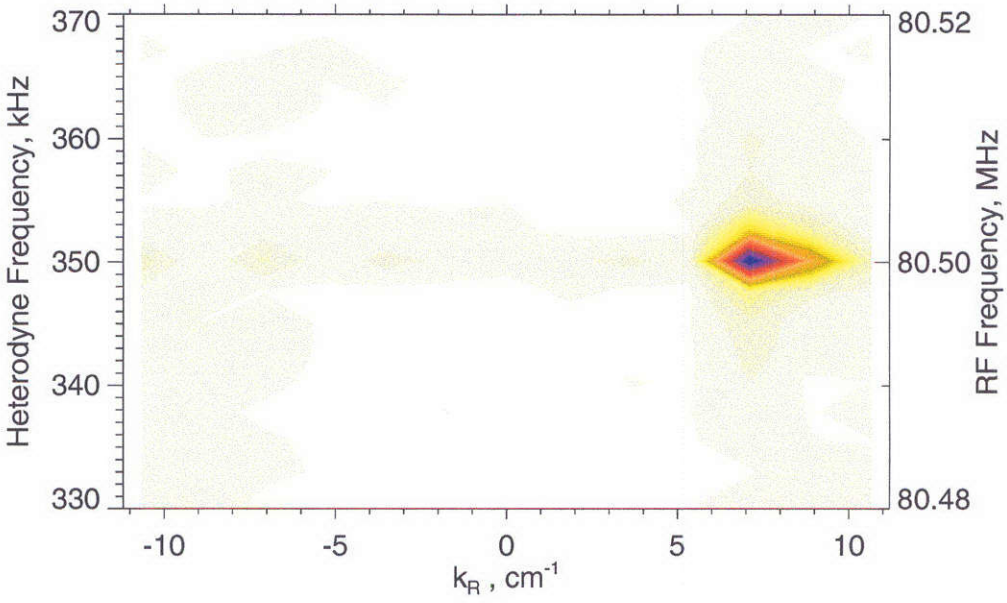

FIGURE 3. Ion Bernstein Wave observation at $k_R = +7\,to\,+9\,cm^{-1}$.

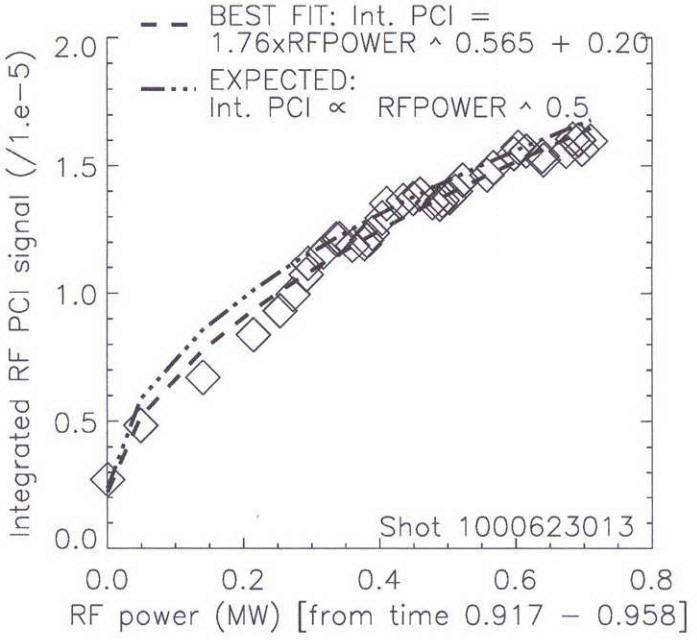

FIGURE 4. RF PCI signal scales with E_{RF} (i.e. $\sqrt{P_{RF}}$).

The antennas launch a bi-directional spectrum of toroidal mode numbers. Each toroidal mode number solution for the RF electric field in the plasma can be treated independently, since n_ϕ is conserved throughout the plasma cross-section. Thus, an estimate can be made of the density fluctuation pattern for a given set of plasma parameters by solving for the electric field of the dominant toroidal mode number

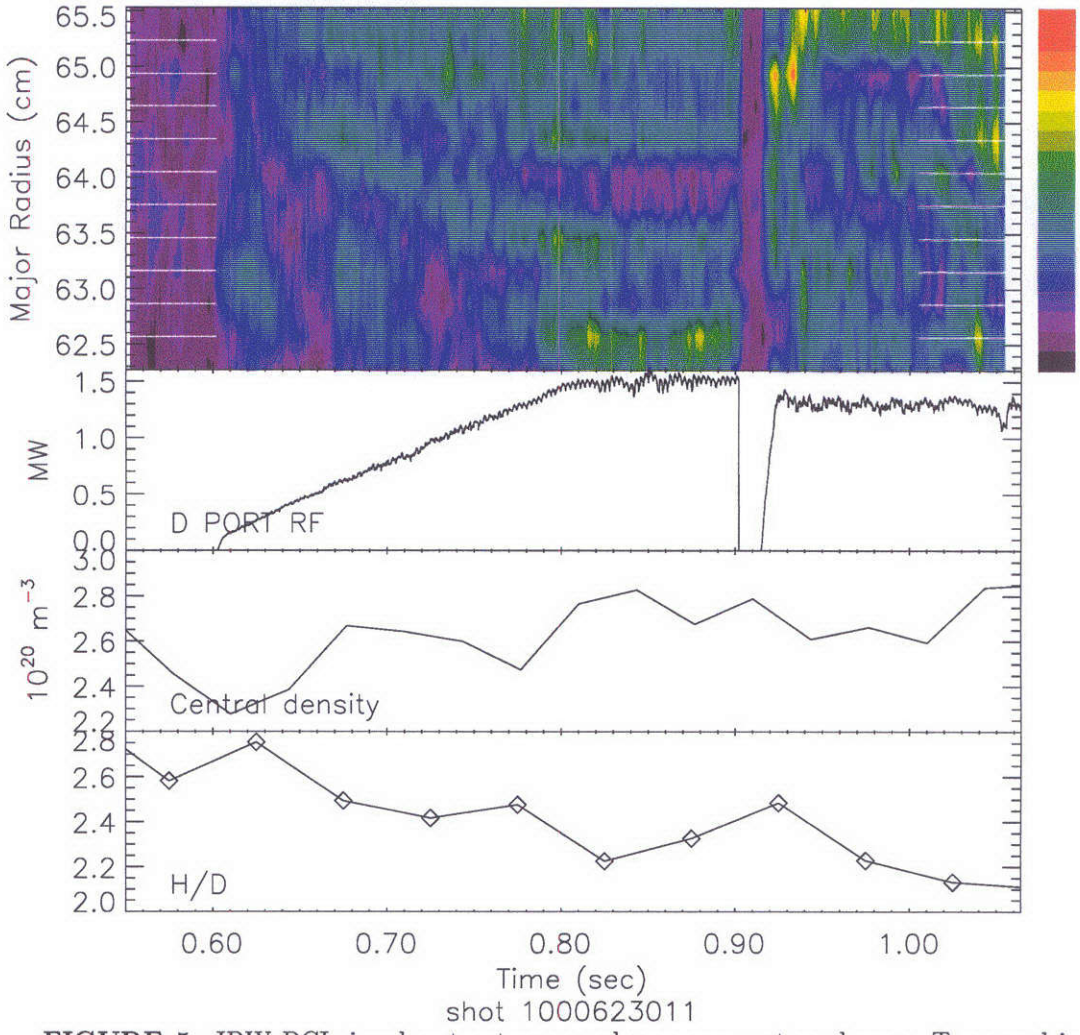

FIGURE 5. IBW PCI signal restructures as plasma parameters change. Top panel is a contour plot of the intensity of all 12 PCI channels (D-port antenna excitation). H/D is the Hydrogen to Deuterium ratio (^{3}He not well known).

launched by the two-strap antenna. Then, using the electron fluid continuity equation and the linearized momentum conservation equation in the cold plasma limit, the solution for the RF fluctuating density n_{e1} can be solved in terms of $E_{RF}, \nabla \cdot E_{RF}$ and B_0. TORIC was run with a set of plasma parameters typical for these 3-species plasmas (5.8 T, 800 kA, 33% H, 23% ^{3}He, 21% D, $2.4 \times 10^{20}\, m^{-3}$, 1.5 keV). Vertical integration of n_{e1} successfully reproduces the general features of the experimental results (See **Fig. 6**). Note the two strong peaks in the line-integrated result between 0 and -2.5 cm, separated by about 1.5 cm. These two peaks are largely due to integrating through the region of large density fluctuation centered around X = -1 cm, Z = -6 cm (with significant contributions from further up as well, up to 10 cm above the midplane). The largest contribution to the electron density fluctuation in this region is from the divergence of the electron velocity, specifically the parallel electron velocity term in the divergence. This explains why it appears similar to the parallel electric field. The strong peak in the line-integrated result

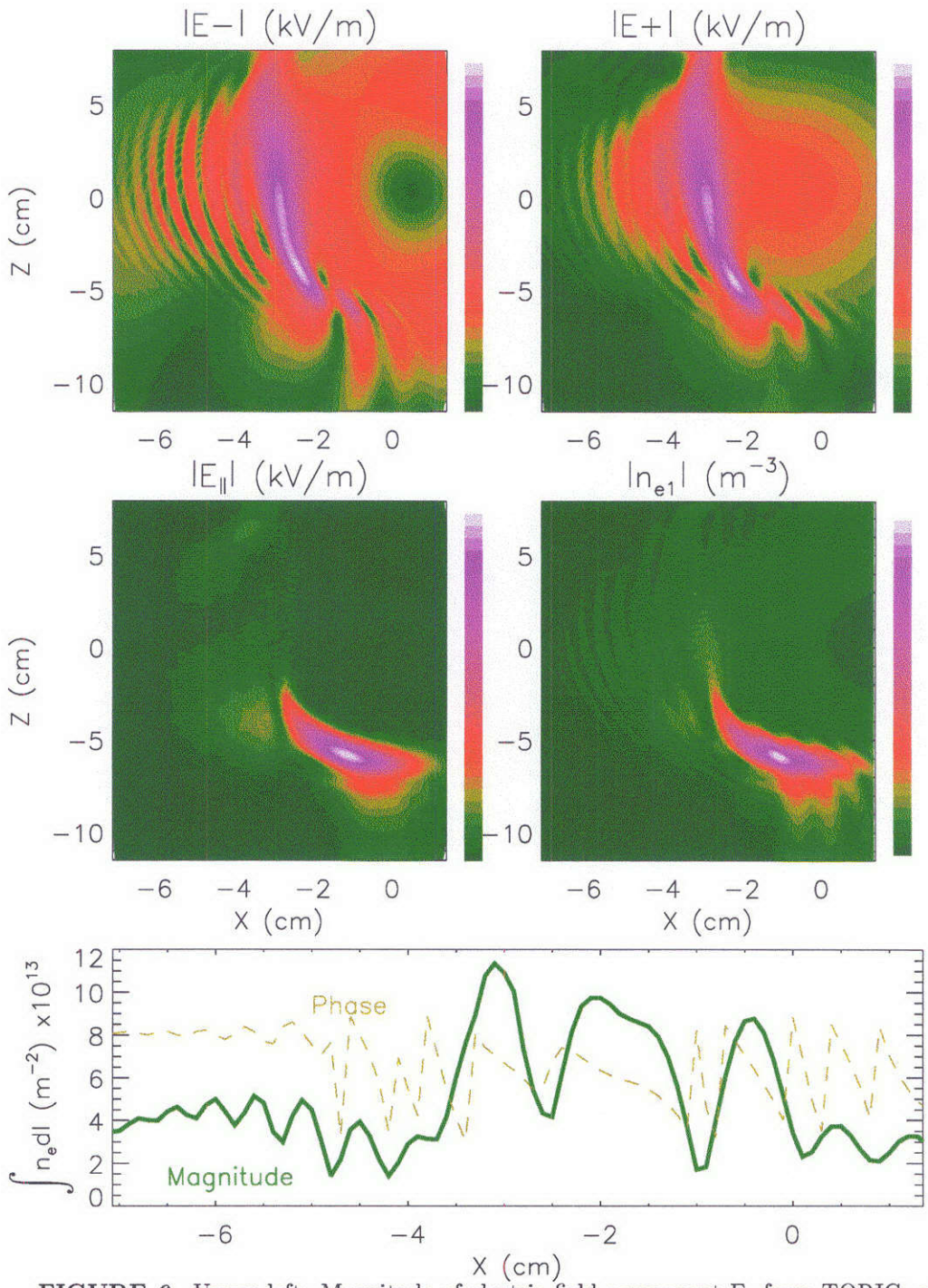

FIGURE 6. Upper left: Magnitude of electric field component E- from TORIC, contour levels from 0.01 to 15.7 kV/m, Upper right: E+ (.01 to 13.5 kV/m), Middle Left: $E_{\|}$ (parallel to total magnetic field) (.00002 to .14 kV/m), all for 500 Amp in the current strap, $n_\phi = 10$. Middle right: Magnitude of RF fluctuating density (using $\vec{E}$ and $\nabla \cdot \vec{E}$) (3.55×10^{12} to 1.13×10^{16}). Bottom: Vertically line-integrated electron density fluctuation.

at -3 cm and subsequent short wavelength peaks out to -6 cm are mostly due to fluctuating electron density that conforms more closely to the E+ and E- electric field pattern.

PCI measurements in these scenarios have generally shown several regions of strong intensity corresponding to IBW wavenumbers (inferred from channel to channel phase advance, or from spatial Fourier analysis) separated by roughly 1 to 2 cm. Note that the fast wave half-wavelength for these shots was approximately 5 cm, so the node/anti-node structure of the fast wave cannot adequately explain these results. The high plasma current shot (1 MA) had a smaller overall extent of strong signal than the average low current (400 kA) shots, perhaps due to more rapid Landau damping at higher current. The exact field pattern and line-integrated signal depends quite sensitively on the exact plasma parameters, so it is not possible at this time to make direct comparisons for a certain plasma at a certain time with a TORIC simulation. It is possible that with further 3-D modelling more experimental features could be explained. This would entail summing many different toroidal harmonic solutions weighted according to their relative power in the antenna spectrum, then looking at a specific toroidal location (0° for E-port or 36° for D-port) in order to see the density fluctuation structure where the PCI is located.

CONCLUSIONS

Fast Waves and Ion Bernstein Waves have been imaged for the first time in Alcator C-Mod. The fast wave has been detected across roughly one entire wavelength and the IBW across several wavelengths, tracing the progress from mode-conversion to damping. Further work in order to compare the absolute amplitude of the RF electric field and mode conversion efficiency with theory will require more detailed 3-D modelling and more complete knowledge of the exact plasma parameters, especially the ^{3}He concentration in the plasma. This could be accomplished in the future with the neutral particle analyzer, diagnostic neutral beam or omegatron diagnostic which will be operational in future runs. Also D(^{3}He) mode conversion scenarios could be further explored and tested to see if the IBW damping lengths are indeed shorter than in these 3 species plasmas, as expected from theory and previous experience.

*Work supported by US DoE Cooperative Agreement No. DE-FC02-99ER54512.

REFERENCES

1. M. Brambilla, *Nucl. Fusion* **38**, 1805-1817 (1998).
2. E. Nelson-Melby, et al., *Bull. Am. Phys. Soc.* **45**, 189 (2000).
3. A. Mazurenko, et al., *Bull. Am. Phys. Soc.* **45**, 318 (2000).
4. P. Lee, et al., *Phys. Rev. Lett.* **49**, 205-208 (1982).
5. H. Park, et al., *Phys. Rev. Lett.* **52**, 1609-1612 (1984).
6. M. Ono, K.L. Wong, G.A. Wurden, *Phys. Fluids* **26**, 298-309 (1983).
7. TFR Group, A. Truc, D. Gresillon, *Nucl. Fusion* **22**, 1577-1587 (1982).
8. Y. Takase, et al., *Phys. Rev. Lett.* **59**, 1201-1204 (1987).
9. K. Ida, M. Naito, S. Shinohara, K. Miyamoto, *Nucl. Fusion* **23**, 1259-1262 (1983).
10. J.H. Lee, et al., *Phys. Rev. Lett.* **80**, 2330-2333 (1998).
11. H. Weisen, *Rev. Sci. Instrum.* **59**, 1544-1549 (1988).
12. S. Coda, PhD Thesis, *An Experimental Study of Turbulence by Phase-Contrast Imaging in the DIII-D Tokamak*, Massachusetts Institute of Technology, (1997).
13. P.T. Bonoli, et al., these proceedings, (2001).
14. C.L. Fiore, et al., *Phys. Plasmas*, **8**, 2023-2028 (2001).